

A Prototype Therapy System for Boiling Histotripsy in Abdominal Targets Based on a 256-Element Spiral Array

Christopher R. Bawiec, Tatiana D. Khokhlova¹, Oleg A. Sapozhnikov²,
Pavel B. Rosnitskiy¹, Bryan W. Cunitz, Mohamed A. Ghanem², Christopher Hunter, Wayne Kreider¹,
George R. Schade, Petr V. Yuldashev, and Vera A. Khokhlova¹

Abstract—Boiling histotripsy (BH) uses millisecond-long ultrasound (US) pulses with high-amplitude shocks to mechanically fractionate tissue with potential for real-time lesion monitoring by US imaging. For BH treatments of abdominal organs, a high-power multielement phased array system capable of electronic focus steering and aberration correction for body wall inhomogeneities is needed. In this work, a preclinical BH system was built comprising a custom 256-element 1.5-MHz phased array (Imasonic, Besançon, France) with a central opening for mounting an imaging probe. The array was electronically matched to a Verasonics research US system with a 1.2-kW external power source. Driving electronics and software of the system were modified to provide a pulse average acoustic power of 2.2 kW sustained for 10 ms with a 1–2-Hz repetition rate for delivering BH exposures. System performance was characterized by hydrophone measurements in water combined with nonlinear wave simulations based on the Westervelt equation. Fully developed shocks of 100-MPa amplitude are formed at the focus at 275-W acoustic power. Electronic steering capabilities of the array were evaluated for shock-producing conditions to determine power compensation strategies that equalize BH exposures at multiple focal locations across the planned treatment volume. The system was used to produce continuous volumetric BH lesions in *ex vivo* bovine liver with 1-mm focus spacing, 10-ms pulse length, five pulses/focus, and 1% duty cycle.

Index Terms—Boiling histotripsy (BH), high-intensity focused ultrasound (HIFU), nonlinear waves, shock front, tight packing non-periodic phased array, Westervelt equation.

I. INTRODUCTION

BOILING histotripsy (BH) is one of the recently developed modalities of high-intensity focused ultrasound (HIFU) designed to mechanically ablate tissue at targeted focal sites without thermal effect [1]–[4]. In BH treatments, millisecond-long pulses (1–10 ms) with high-amplitude shock fronts (>60 MPa) are delivered to the focus at low duty cycles of about 1%. The shocks are formed in the acoustic waveform due to nonlinear propagation effects and are present only in the focal region of the HIFU beam [5]. Pulse duration is chosen so that tissue is heated to a boiling temperature within each pulse resulting in the generation of an mm-sized vapor bubble at the focus [6]. Interaction of the remaining cycles of that pulse with the vapor cavity causes tissue liquefaction through mechanisms known as acoustic atomization, microfountaining, and subsurface cavitation [7], [8]. This approach has promising clinical benefits over currently used HIFU thermal therapies: BH treatments can produce precisely controlled mechanical lesions with sharp margins and selective sparing critical structures, such as blood vessels [2], [9]. Ultrasound (US) imaging can be used for treatment targeting and monitoring in real time, as well as for the evaluation of outcomes [10]. Finally, the nonthermal nature of BH eliminates heat sink effects that occur in well-vascularized targets in thermal therapies and diminishes the risk of thermal damage to bones and overlying tissues [11].

BH is being explored for various clinical applications involving tumors in the prostate [12]; tumors and hemorrhages in the brain [13]; cancer vaccines and immunomodulation [14]–[16]; stimulation of cancer biomarker release [17]; tissue decellularization for regenerative medicine [2], [9]; and liquefaction of large hematomas [18]. Our group has been evaluating the feasibility of US-guided BH for the ablation of targets in abdominal organs—in particular, liver and kidney. Successful transcuteaneous and partially transcostal generation

Manuscript received August 27, 2020; accepted November 3, 2020. Date of publication November 6, 2020; date of current version April 26, 2021. This work was supported in part by the National Institutes of Health under Grant R01EB007643, Grant R01EB025187, and Grant PO1 DK043881 and in part by the Russian Science Foundation under Grant 19-12-00148. (Corresponding author: Vera A. Khokhlova.)

Christopher R. Bawiec and Tatiana D. Khokhlova are with the Division of Gastroenterology, University of Washington School of Medicine, Seattle, WA 98195 USA (e-mail: cbawiec@medicine.washington.edu).

Oleg A. Sapozhnikov and Vera A. Khokhlova are with the Physics Faculty, Moscow State University, 119991 Moscow, Russia, and also with the Applied Physics Laboratory, Center for Industrial and Medical Ultrasound, University of Washington, Seattle, WA 98105 USA.

Pavel B. Rosnitskiy and Petr V. Yuldashev are with the Physics Faculty, Moscow State University, 119991 Moscow, Russia.

Bryan W. Cunitz, Mohamed A. Ghanem, Christopher Hunter, and Wayne Kreider are with the Applied Physics Laboratory, Center for Industrial and Medical Ultrasound, University of Washington, Seattle, WA 98105 USA.

George R. Schade is with the Department of Urology, University of Washington School of Medicine, Seattle, WA 98195 USA.

Digital Object Identifier 10.1109/TUFFC.2020.3036580

of volumetric BH lesions in porcine liver and kidney has been demonstrated *in vivo* using the mechanical translation of a single-element HIFU transducer to move its focus over a trajectory of discrete sonication points [11]. This experiment also revealed challenges that need to be addressed before clinical implementation of BH. Respiratory motion interfered with precision and uniformity of ablation in some of the targets and the need for mechanical translation of the focus exacerbated the problem. Complex randomized focus translation trajectories similar to those used in clinical HIFU systems could not be realized using mechanical translation alone [9]. Furthermore, inhomogeneities of the body wall introduced aberrations that resulted in degradation of the focus requiring a significant increase in the acoustic power to achieve BH conditions at the target site.

The use of multielement focused phased arrays in transcutaneous US-guided BH treatments provides the potential for electronic steering to compensate for respiratory motion by rapidly changing the focus location. In addition, element phases can be adjusted for aberration correction [19]–[24]. In particular, the use of rapid electronic focus steering for volumetric BH ablation of *ex vivo* tissues was recently demonstrated with a phased array of MR-guided HIFU system (Sonalleve V1, Profound Medical, Ontario, CA, USA) [9]. These recent *in vivo* and *ex vivo* studies motivated the design, fabrication [25], and initial characterization [26] of a 256-element HIFU array of 1.5-MHz frequency for abdominal US-guided BH application.

Various types of therapeutic array systems with either MR or US guidance have been previously developed for specific clinical indications and HIFU methods, including thermal ablation and piezoelectric lithotripsy [27]–[29]. The design of the prototype developed here reflected the specific requirements for treating abdominal targets with BH. First, a high filling factor was necessary to achieve peak power levels typical for BH exposures, which was addressed by using a new compact multiarm spiral design of the array with minimized interspaces between its elements. This provided a filling factor of about 60% compared with about 35%–40% for the most existing random or spiral array systems of similar frequency and geometry [27], [28], [30]–[31] and similar to the highly compact quasi-random array of a clinical MRgFUS system [32]. The nonperiodic spiral pattern of the array also enhanced its steering capabilities by reducing grating lobes. The second requirement to the system was the capability of generating shocks over 80-MPa amplitude at the focus *in situ* without exceeding technological intensity limitations at the array surface of 30 W/cm² for pulses of up to 10-ms duration. Multiparametric simulations have been performed in our previous studies to determine a combination of the focusing angle and array aperture to satisfy these requirements [25], [33]. The third requirement to the system was the ability for electronic focus steering in the shock-forming regime to generate volumetric BH lesions. Thus, the electronic steering procedure providing equalized parameters of the shocked waveform at the steered foci had to be developed and validated.

More complex high-power multichannel electronics had to be employed to drive the array compared with single-element

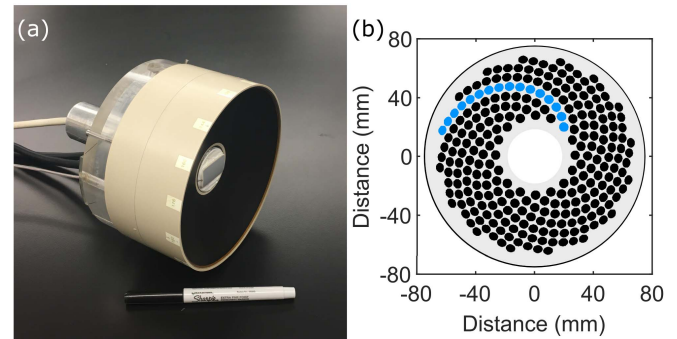


Fig. 1. (a) Photograph of the 256-element HIFU array with a US imaging probe (ATL P6-3) inserted into the central opening of the array. (b) 2-D projection of the layout of array elements with one of the 16 spirals shown in blue for illustration.

transducers. This effort, therefore, included the following steps toward future preclinical and clinical studies that utilize BH for target sites in kidney and liver: implementation and characterization of a US-guided phased-array BH system in combination with development and testing of shock-wave exposure protocols for liquefying *ex vivo* tissue volumes using electronic focus steering. Note that, while US guidance is an essential part of the system, the emphasis of this work was on the therapy component, and B-mode US imaging was used in the same capacity as in our prior work [11].

II. MATERIALS AND METHODS

A. HIFU Transducer and Driving Electronics

The HIFU transducer was a 1.5-MHz, 256-element geometrically focused array fabricated from a composite material (Imasonic, Voray sur l'Ognon, France). The array had a nominal focal distance of 120 mm, an outer diameter of 144 mm, and a 40-mm central opening for treatment monitoring with a coaxially aligned US imaging probe, as shown in Fig. 1(a). The elements of 7 mm in diameter with a minimum spacing of 0.5 mm between them were arranged in a 16-spiral configuration with 16 elements per spiral [see Fig. 1(b)]. As mentioned previously, such dimensions and arrangement of the elements were chosen to achieve a nonperiodic element pattern while maximizing the filling factor.

The array was specifically designed to have sufficient steering capabilities and be able to generate high-amplitude (>100 MPa) shock fronts at the focus without exceeding technological limits of acoustic intensity (30 W/cm²) at the element surfaces [25]. The total area of all array elements was 98.5 cm², and thus, the maximum safe peak acoustic power was about 3 kW. With nominal 63% electroacoustic efficiency of the transducer and ideal matching of each element to the channels of the driving system, up to 5-kW electrical power of the system would be needed to reach the maximum safe acoustic power for the array.

The array had two connectors that were attached to a Verasonics research US system (V-1 Ultrasound Acquisition platform, Verasonics Inc., Kirkland, WA, USA) via a custom matching network. The mean impedance of all 256 channels of the array was 59.1–207.9 j Ω. Since the real part of the impedance was close to 50 Ω, a series inductor was selected

to cancel the imaginary component of the impedance at 1.5 MHz (SRR1005-270Y Bourns, Riverside, CA, USA). The inductor was selected to be compact, shielded, and handle the required current and voltage without saturation. Two four-layer circuit boards were designed so that 64 inductors could be surface mounted on each side. Each board, thus, received input connections from 128 elements of the array and provided corresponding outputs to the Verasonics system with a final impedance of $72.2 + 13j \Omega$.

The Verasonics four-board V-1 system with a HIFU option included an external 1200-W dc power supply (QPX600DP, Aim-TTI, Huntingdon, U.K.) with both dc output channels connected in parallel to allow for greater source current. The system was modified from its retail configuration with the addition of seven electrolytic capacitors identical to the internal dc supply capacitor of the system (B41560A9159M000, EPCOS, Munich, Germany). One of the capacitors was installed internally; the other six were mounted in a separate box external to the V-1 system in parallel with the dc power supply. The addition of the capacitors allowed for sustained delivery of the 5-kW electric power for up to 10 ms at a duty cycle of no more than 2%. To ensure that the extra sustained current would not damage components of the Verasonics system, the software script “TXEventCheck.m” was modified to account for hardware changes and estimate the new output limits. It was determined that the maximum safe element driving voltage with the new capacitors was $43 V_{\text{peak}}$ (corresponding to 3.7-kW total electric power delivered into the transducer) for 10-ms pulses. A more detailed description of the impedance matching of the array with the Verasonics system has been reported in [26], where the array performance was characterized at low operational levels and used to generate vortex beams. Also, note that the developed high-power Verasonics driving system could be used to drive a multielement array of any other design, provided the electrical matching and an appropriate number of elements.

Different software interfaces were implemented for controlling the system to operate the HIFU array during hydrophone measurements and BH treatments. They allowed manual selection of the number of cycles per pulse, the pulse repetition frequency (PRF), the electronic steering location of the focus, and the voltage of the dc power supply used to control the acoustic output of the transducer (referred to, hereafter, as the driving voltage). Hydrophone measurements in the near field of the array were used to generate calibration voltage–pressure curves. For steering, the desired location of the focus was chosen, and the corresponding time delays at each array element were calculated and implemented by the system. For tissue treatments, US pulses were delivered by triggering the system with a 1-Hz square wave input. Other interfaces were implemented to enable automated treatment of tissue volumes by using custom scripts in which all variables were preprogrammed, including the trajectories of discrete translation of the HIFU focus.¹

¹The scripts developed and used in this work are available upon request.

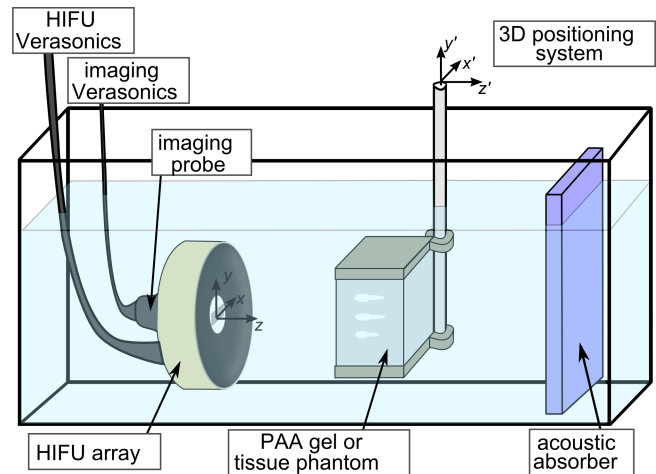


Fig. 2. Experimental setup for acoustic characterization of the system, visualizing lesion formation in polyacrylamide gels, and US-guided generation of BH lesions in gel and *ex vivo* liver samples. For acoustic measurements, a gel/tissue holder attached to the 3-D positioning system was substituted by either a PVDF capsule hydrophone or a fiber optic probe hydrophone that was used at low and high driving voltages applied to the array. The axes of the array $\{x, y, z\}$ were made parallel to the axes of the positioning system $\{x', y', z'\}$.

B. Experimental Arrangements

A diagram of the experimental setup is shown in Fig. 2. All acoustic measurements were performed at room temperature in a tank filled with deionized, degassed water. The dissolved oxygen content was kept below 25% and was as low as 10% when operating at high driving voltages as measured by a dissolved oxygen meter (WTW Oxi 330i, Weilheim in Oberbayern, Germany). To synchronize the data acquisition, a function generator (Model 3500B, Keysight Technologies Inc., Englewood, CO, USA) triggered both the Verasonics system and a 14-bit digitizer board (Razor 14, Gage by DynamicSignals LLC, Lockport, IL, USA) that were used to record hydrophone signals. Holders used for either hydrophones or target samples of gel/tissue were connected to a computer-controlled positioning system with three linear axes (Velmex Inc., Bloomfield, NY, USA).

The HIFU array elements were all driven with identical electrical waveforms where only the timing of a pulse was slightly adjusted per element so that all the acoustic waves arrived in the geometric focus at the same time. The “baseline” timing delays were established during previous work to account for the differences in element placement that occurred during manufacturing [26]. These delays were on the order of tens of nanoseconds. In order to change the position of the focus of the HIFU transducer array, electronic beam steering was implemented by choosing additional time delays for each individual element so that the arrival time of the wave from each element was the same at the target location. This enabled steering of the HIFU focus both laterally and axially. At low driving voltages that yielded peak focal pressures below 2 MPa, free-field measurements were performed using a calibrated PVDF capsule hydrophone, HGL-0085, with an AG-20 $\times 0$ preamplifier (Onda Corporation, Sunnyvale, CA, USA). The hydrophone sensitivity provided by the manufacturer was 416 mV/MPa at 1.5 MHz. The hydrophone directivity at

1.5 MHz measured in our earlier study was used to provide corrections to the field measurements [26]. At higher driving voltages, the field was measured using a fiber-optic probe hydrophone with 100-MHz bandwidth (Model FOPH 2000, RP Acoustics, Leutenbach, Germany).

C. Acoustic Field Characterization With No Steering

We first characterized array performance with no steering, following our previously developed approach that included holography measurements, pressure output calibration over a range of driving voltages, and nonlinear modeling [32]. Then, we investigated how beam steering in transverse and axial directions affected the relative array performance.

Three sets of hydrophone measurements were performed in water at low-pressure amplitudes. One set utilized measurements at a single near-field point (on-axis, 40-mm prefocal) to characterize the output acoustic power across a range of driving voltages from 1.6 to 35 V. The second set involved holography measurements made in a prefocal plane at a driving voltage of 10 V. These two sets of measurements were used to reconstruct source vibrations and define boundary conditions for use in simulations. The third set of measurements involved linear scans through the geometrical focus of the array at a driving voltage of 1.6 V and was used to provide a check on the stability and accuracy of holography measurements.

Holography measurements were recorded 40-mm proximal to the focus of the array in a scan plane with an aperture of 88×88 mm and a step size of 0.5 mm [34], [35]. An effort was made to position the array so that its z -axis was coincident with a horizontal axis, z' , of the positioning system (see Fig. 2). Pulses lasting 128 cycles were excited, and eight cycles of the measured pressure waveform were analyzed starting 120 μ s after the pulse was triggered. Raw hydrophone measurements were corrected for hydrophone directivity by applying a 2-D fast Fourier transform (FFT) and introducing a factor to correct the amplitude of each plane wave according to its angle of incidence with the hydrophone [26]. By integrating the wave intensity over the holography plane, the hologram corrected for directivity was used to calculate the actual acoustic power delivered by the array for comparison with simulations. Similarly, the third set of measurements recorded in the focal region was corrected to account for hydrophone directivity. Toward this end, two vibrational patterns of the surface of the array were reconstructed from the raw and corrected holograms. Corresponding values of acoustic pressure at the focus of the array were calculated using the Rayleigh integral approach [32], [35]. The ratio of the focal pressures obtained using the corrected and raw holography data was then calculated and used as a correction factor to the nominal sensitivity of the hydrophone in the focal region of the array.

The boundary condition to the nonlinear Westervelt model was set at the plane ($x, y, z = 0$) at the apex of the array as a pressure distribution determined from the holography measurements. The angular spectrum method was used to linearly backpropagate the field represented by the corrected hologram. The magnitude of this pressure distribution was scaled based on the near-field power characterization measurements.

Nonlinear modeling of the full 3-D field generated by the array transducer then was performed for different array output levels. A detailed description of the numerical algorithm and its validation for various transducers has been presented in our earlier articles [32], [33], [36]. Focal waveforms obtained in the modeling were compared with those measured by the FOPH to obtain the set of peak pressures and shock amplitudes that are reached at the focus of the array. For these validation studies, both measurements and simulations were collected at the location of the maximum peak positive pressure, p^+ , at 15 V.

D. Acoustic Field Characterization With Steering

Electronic steering capabilities of the array were characterized for both low-pressure (linear) focusing conditions and high-pressure (nonlinear) conditions for which shock fronts form at the focus.

Low-pressure measurements were performed with the capsule hydrophone at a 1.6-V output level for different steered locations. Initially, the hydrophone was placed in the geometrical focus of the array and then the raster scanned across the focal region recording 125 cycle pulses at every point. Lateral scans in both the horizontal x -direction and vertical y -direction (see Fig. 2) were performed with a 200- μ m step. For the axial scans along the z -direction, a 500- μ m step was used. This was done for each steering location in two transverse coordinates in the plane of the geometric focus of the array and axially. Simulations were performed by assuming that the transducer vibrations are defined by the element design geometry and uniform vibration of each element. The open-source software, T-array, specifically developed for analyzing linear steering capabilities of therapeutic arrays with circular elements was used in the simulations [37].

For shock-forming focusing conditions, the focus was first steered to the desired location, and the FOPH hydrophone was scanned through the pressure field at a 15-V driving level to identify the position of the maximum of peak positive pressure p^+ . Once this maximum location was identified, the dc driving voltage set on the Verasonics power supply was increased from 2 to 20 V in 1-V increments. The array was driven with 32-cycle pulses at a PRF ranging from 1 to 10 Hz. The lower amplitude signals (up to 12 V) were averaged eight times; from 13 to 17 V, the readings were averaged four times, and the readings taken over 17 V were not averaged. The reason for the different number of averages was that cavitation was a common occurrence at higher pressure levels ($|p_-| > 18$ MPa), making it technically difficult to accurately average the signals. These measurements were performed at lateral steering positions ± 6 mm in the focal plane and at axial prefocal (-14 mm) and postfocal ($+10$ mm) positions.

After collecting the acoustic waveforms acquired at the different steering positions, the waveforms were analyzed to determine the input voltage level required to generate shocks of the same amplitude of 80 MPa. This shock amplitude was chosen based on being sufficient to achieve boiling temperature within 5 ms in tissue, which, in turn, would facilitate initiation of BH with 10- ms pulses [1], [38]. After determining the necessary input voltage, hydrophone scans were performed

at this voltage axially and laterally to the steered focus. The scans consist of 32 cycle pulses every second averaged eight times per location with 50- μm step size in the lateral direction and 250- μm step size in the axial direction.

E. Gel Phantom Experiments

Optically transparent 5% polyacrylamide gel phantoms (without the addition of bovine serum albumin) with acoustic properties very similar to water [1], [39] were prepared for visually assessing the BH lesions generated in gels at different focus steering locations. The gels were prepared the same day as the experiments and stored in plastic molds of 55 mm \times 55 mm \times 65 mm size until they were ready to use. For the experiments, the gels were placed in a custom 3-D-printed holder, which secured them from the top and the bottom without interfering with the HIFU beam (see Fig. 2), and the holder was attached to the 3-D positioning system. The gel was positioned with one side perpendicular to the z -axis of the array. The array's geometric focus was located at 15-mm depth within the gel when steering the focus -10 mm prefocally and at 10-mm depth for other steering configurations.

A Verasonics interface was used for delivering sets of up to 30 pulses of 10-ms duration, once per second, to a certain electronically steered focal location. The output voltage was first set slightly below the level at which boiling was predicted to occur based on the FOPH measured waveforms and then gradually increased with a 0.2-V step. When boiling was initiated at the focus within a pulse, the focal region became opaque due to the disruption of polyacrylamide structure by a vapor bubble. The presence of this region, therefore, indicated the voltage threshold for BH initiation at the current focal steering location. The focal steering locations tested were -6 to 6 mm in 2-mm increments laterally (in both x - and y -directions) and -10 mm prefocally to $+15$ mm postfocally in 5-mm increments axially. The voltage threshold for lesion generation at each steered location was tested a minimum of five times with a minimum spacing between the lesions of 4 mm.

Once the dc voltages required to produce individual BH lesions in the gel with 10-ms pulses were established, scripts were developed with the required voltage for each focal steering position preprogrammed. With the intent of treating a volume, automated scripts steered the focus over planar trajectories, with larger volumes, including multiple treatment planes spaced 5 mm apart along the beam axis. In each plane, trajectories comprised multiple concentric circles with radii of 2, 4, and 6 mm. Within each circle, the tangential spacing between target sites was approximately 1.5 mm (49 focus locations per plane) [9], [19]. To ensure uniform BH lesion formation across the characterized range of focal steering, 10-ms BH pulses were delivered to the polyacrylamide gel over the entire volumetric trajectory described earlier. In every plane, each point of the trajectory received one BH pulse and then the process was repeated until overall 30 pulses per point were delivered. In addition, each concentric ring, starting from the center outwards, was treated such that the sonication points alternated from one side of the circle to the other to minimize heat buildup. If multiple planes were treated, then the furthest

plane from the transducer was treated first, followed by the next closest.

F. Liver Experiments Ex Vivo

The fresh bovine liver was obtained from a nearby abattoir on the first day of the experiments, and all testing occurred within 55 h from the receipt. The liver was kept on ice in a cooler during transport to the laboratory and placed into a refrigerator before the experiment. To prepare the samples for treatment, 3-5-cm-thick sections of the liver were excised, with surfaces of approximately 8 cm \times 8 cm, one or two of which included liver capsule. Care was taken to avoid large vessels in the samples to obtain a relatively homogeneous tissue volume. Each sample was placed in a container with phosphate-buffered saline (PBS) solution and degassed under vacuum for one hour at room temperature right before use. For the experiments, the liver samples were secured in a custom holder attached to the 3-D positioning system similar to that used for the gels (see Fig. 2).

The driving voltage required to generate BH in the liver at each steering location was determined by scaling the voltages obtained from the gel measurements [40] to account for the difference in acoustic attenuation in the gel (negligible) and liver ($\alpha = 0.07$ Np/cm at 1.5 MHz) [38], [41], [42]. Knowing the treatment depths in the tissue, the driving voltages were increased by the factor of $\exp(\alpha \cdot \Delta z)$ for treatment depths of $\Delta z = 5, 10,$ and 15 mm, resulting in voltage increases of 3%, 7%, and 10%, respectively. The occurrence of BH within the liver was also confirmed with coaxial US B-mode imaging as the appearance of a bright hyperechoic region corresponding to the presence of bubbles at the focus [10], [11], [38]. The US imaging probe (ATL P6-3) was connected to a separate Verasonics V-1 system and was continuously performing B-mode imaging during BH exposures. Since only the bubbles produced within the azimuth plane of the imaging probe were visible with B-mode, the initiation of BH was identified only at laterally steered positions of the focus along the horizontal x -axis (see Fig. 2). Therefore, before implementing volumetric treatments, individual BH lesions were tested in the liver for combinations of steering locations in the x -direction (0, 2, 4, and 6 mm) and in axial steering locations ($-5, 0,$ and 5 mm from the geometrical focus).

For the first set of volumetric liver treatments, the same circular trajectory was used for each lateral plane as in the gel experiments. For the second set, the points constituting the trajectory were spaced 1 mm apart, both radially and circumferentially, resulting in 136 locations per treatment plane. For steering locations existing geometrically between the tested focus locations (i.e., for concentric rings with radii of 1, 3, and 5 mm), the dc voltage value used was always the higher voltage value. The axial planes treated in both sets were $+5$ -mm postfocal, focal, and -5 -mm prefocal, which constitutes a treatment volume of approximately 2 cm³. All treatments of the liver were performed with the geometric focus of the array placed 10 mm inside the liver sample. Three planes were treated consecutively beginning with the plane furthest from the transducer. Each focal point in each plane received a single BH pulse before repeating the sonication, for

up to 30 total pulses per location (first set) or up to ten pulses per location (second set).

After the treatment, the samples were bisected in the plane perpendicular to the HIFU propagation axis at 10-mm depth below the liver capsule to assess the degree of tissue liquefaction. Following bisection, the volumes were photographed, then flushed with PBS to remove the liquefied contents, and photographed again.

III. RESULTS

A. HIFU Transducer Array and Driving Electronics

Prior to the after-market modifications to the Verasonics system, the BH capabilities of the HIFU array were limited by the dc voltage supply being unable to provide enough current to the amplifiers for maintaining the required voltage over a duration of 10 ms. Especially, when testing a 1.5-MHz, 10-ms pulse, into a 50- Ω load with the system voltage set to 50 V, a single channel showed the decay of the peak voltage amplitude of the sinusoidal signal from 44 to 21.4 V over the pulse duration. This over 50% reduction in signal amplitude caused by an inadequate supply current made it impossible to perform repeatable BH exposures. After adding the capacitor bank to the system, the same 10-ms pulse exhibited less than 5% voltage decay, thus enabling BH sonications.

The system was tested and validated for delivering 1.5-MHz, 10-ms pulses up to a maximum system driving voltage of 43 V, which is equivalent to approximately 15-W electric power per element. The pulse-average electrical power delivered into the array at the maximum tested level was as high as 3.7 kW. With 63% nominal electroacoustic efficiency of the array, this resulted in a maximum achievable pulse-average acoustic power of 2.2 kW, which corresponds to an acoustic intensity at the array elements of 22 W/cm² (well within safety limits for operating the array).

B. Acoustic Field Characterization With No Focus Steering

A source hologram was reconstructed from the measured hologram corrected for hydrophone directivity. The resulting magnitude and phase of the normal vibrational velocity at the array surface are depicted in Fig. 3 using coordinates aligned to the transducer. Based on the pattern of the reconstructed phase, the angle between the axes of the array and the scan plane defined by the positioner was determined to be less than 0.5°, which confirms good alignment. In the source hologram, all individual elements vibrate with approximately uniform amplitude and phase distributions, which confirms the expected performance of the array.

Forward propagation of the measured hologram was used to determine the 3-D structure of the linear acoustic field in the focal region. Holography-based calculations are compared in Fig. 4 against independent hydrophone measurements through the focus at a system driving voltage of 1.6 V, as well as simulations based on the nominal array geometry with uniformly vibrating elements. Holography projections were scaled from 10-V driving voltage to 1.6 V using the near-field power calibration shown in Table I. In addition, Table I shows the

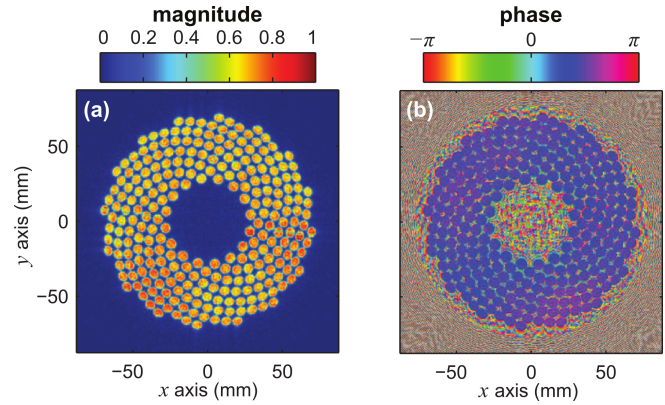


Fig. 3. Reconstruction of normal velocity. (a) Magnitude and (b) phase representing a source hologram defined on the array surface.

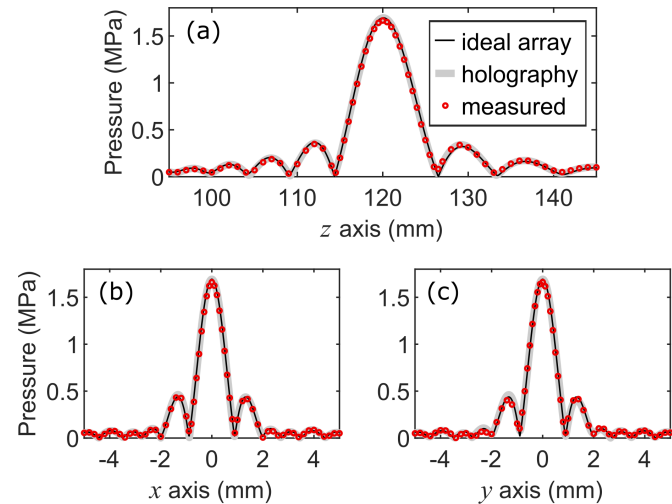


Fig. 4. Linear calibration results. (a)–(c) Comparison of pressures near the focus as measured directly (red circles), projected from the measured hologram (black line), and projected from an idealized representation of the array (gray line). Note that the hologram and direct measurements were corrected for the hydrophone directivity.

nominal intensity I_0 and nominal surface pressure amplitude calculated as $p_0 = \sqrt{2I_0\rho c}$ at a single array element. These parameters were defined by matching the linear focal pressures generated by an idealized array with uniformly vibrating elements to those based on the holography measurements and dividing the total power of this idealized array by 256. To account for directivity in the independent hydrophone scan measurements, the nominal hydrophone sensitivity was scaled by a factor of 1.12. This scaling factor was determined as the ratio of pressure magnitudes at the focus obtained using corrected and raw holography data.

Although the simulation results shown in Fig. 4 are presented in the x , y , and z coordinates of the array and measurements data—in the coordinates of the positioner system, the beam pattern widths and the locations of the nulls along the array axis and transverse coordinates in the focal plane match almost exactly. The length of the focal lobe of the linear beam at the -6 -dB level is 7.2 mm, and the width in both transverse directions in the focal plane is 1.1 mm. Good agreement of simulations and measurements shows that the array operates according to its design and validates the source hologram for use as a boundary condition to the nonlinear modeling.

TABLE I
CALIBRATION OF THE ACOUSTIC OUTPUT OF THE ARRAY
VERSUS DC DRIVING VOLTAGE

DC Volts	Measured acoustic power (W)	Nominal acoustic power (W)	Nominal surface intensity I_0 (W/cm ²)	Nominal surface pressure p_0 (bar)
1.6	1.3	1.3	0.01	0.20
10.0	105.7	106.8	1.08	1.80
15.0	251.3	253.7	2.57	2.78
18.0	367.7	371.2	3.77	3.36
20.0	456.8	461.2	4.68	3.75
35.0	1419.3	1433.1	14.55	6.61

The nonlinear acoustic field produced by the array in the water at different output levels was modeled based on the 3-D Westervelt equation [32], [33], [36], [43]. The boundary condition to the model was scaled in magnitude from the source hologram according to the near-field calibration measurements (see Table I). Simulation results were compared with the FOPH measurements at the focus. The focus location was determined as a spatial maximum of peak positive pressure at 15-V dc. Peak positive and negative pressures are plotted in Fig. 5 over the range of the measured output levels shown here in terms of the system driving voltage. Experimental data were analyzed by averaging peak values over eight acoustic cycles within the steady-state portion of the pulse reached after 20 first cycles; mean values are plotted as circles; and error bars correspond to standard deviation. Simulations and measurements show very good quantitative agreement for the peak positive pressure over the whole range of the driving voltages and for the peak negative pressure within 1–15 V. At higher driving voltages, there is an increasing uncertainty of measured peak negative pressure and deviation from modeling by 15%–20%. This disagreement was likely due to cavitation occurring at the tip of the FOPH hydrophone toward the end of each HIFU pulse when the steady-state output was also reached. Cavitation is known to hinder the precise measurement of high peak negative pressures, especially for pulses longer than a few cycles [44]. Peak positive pressure tracks the formation of shocks as indicated by the steep slope in the curve between 10- and 15-V driving voltages. Several representative simulated focal waveforms are presented in Fig. 6, showing good agreement with the FOPH data for both quasi-linear (at 5 V) and shocked (at 15 and 20 V) waveforms. Shock amplitude calculated from the modeled waveform is 80 MPa at 15 V, and a fully developed shock of 125-MPa amplitude forms at 20 V and then grows up to the maximum value over 150 MPa at the voltage of 35 V.

C. Acoustic Field Characterization With Steering

The results of simulating and measuring the lateral and axial limits of focus steering for the array operating at low driving voltages are presented in Fig. 7. Multiple field simulations were performed assuming linear focusing conditions and nominal parameters of the array. The maximum pressure amplitudes were calculated for various focus locations steered electronically in an axial plane of the array [see Fig. 7(a)] and

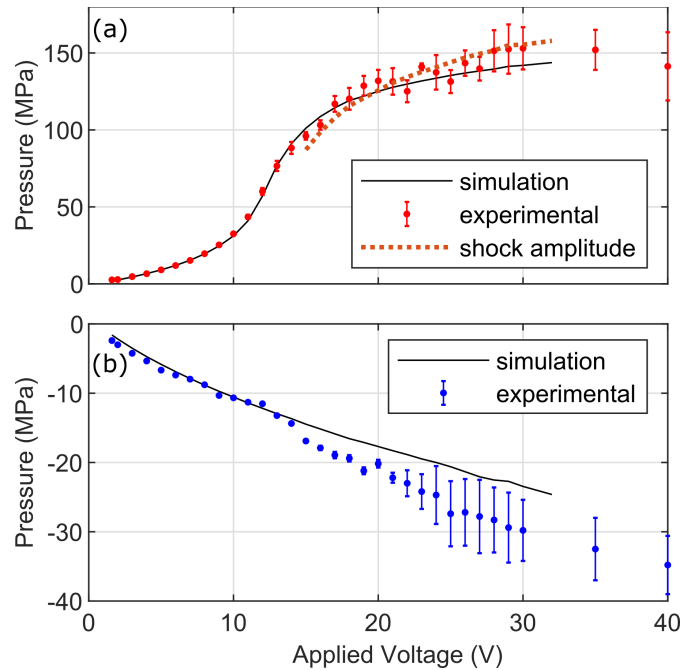


Fig. 5. (a) Peak positive (red) and (b) peak negative (blue) pressures versus system driving voltage values measured at the focus. Error bars correspond to the standard deviation within the measured pressures over the steady-state portion of the pulse. Thin black curves represent the corresponding simulation results for the peak positive and peak negative focal pressures (black); dotted curve (orange) in (a) depicts the simulated shock amplitudes in the focal waveform.

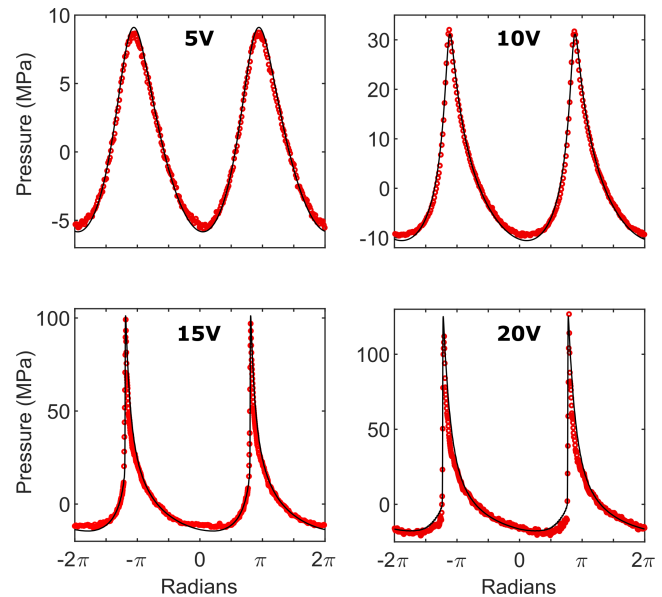


Fig. 6. Simulated (solid black curves) and experimental (red dots) pressure waveforms obtained at the focus at specific system driving voltages.

in the focal plane at $z = 120$ mm [see Fig. 7(b)]. Hydrophone scans were performed along three axes when steering the focus through the nominal focal position in the three directions [see Fig. 7(c)–(e)]. The coordinate along only one axis was varied at a time; the other two coordinates remained at the focus. For the axial steering scans, both simulations and measurements showed that the maximum pressure was achieved when steering 4.5 mm prefocally. A 50% drop in the focal pressure,

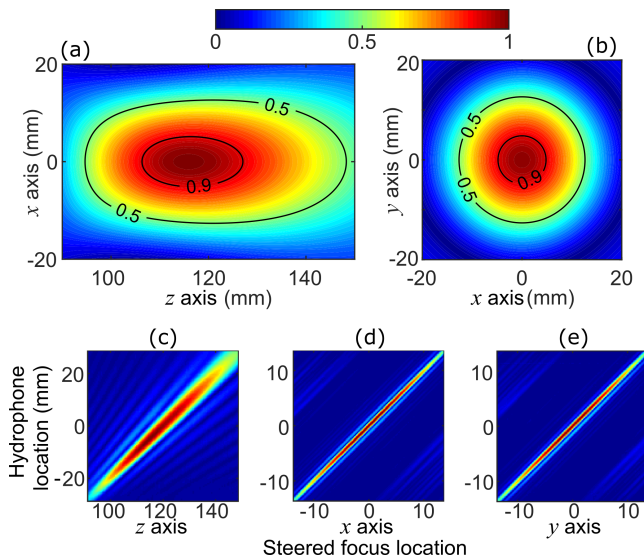


Fig. 7. Simulated pressure amplitudes at electronically steered foci normalized to the maximum achievable pressure in (a) axial plane of the array and (b) transverse plane through the nominal focus at $z = 120$ mm. (c)–(e) Normalized pressure amplitudes obtained from scanning the hydrophone through electronically steered foci along the three axes. In each of (c)–(e), only one coordinate of the steered focus was varied at a time. Electronic steering and hydrophone position along (c) array axis, z , (d) horizontal axis, x , and (e) vertical axis, y .

compared with this maximum achievable value, corresponds to the -25 -mm prefocal and $+28.5$ -mm postfocal positions steering from the nominal focus. The corresponding values for a 10% drop in pressure are -14 and $+10$ mm from the focus. For transverse steering in the focal plane at $z = 120$ mm, a 50% drop in pressure occurred at approximately ± 13 mm and a 10% drop at ± 6 mm in both transverse directions compared with the pressure amplitude at the geometrical focus. Note that the range of the safe focus steering defined by the maximum level of intensity in the grating lobes less than 10% of the intensity at the steered focus [45], [46] is significantly larger than the corresponding values for a 10% drop in pressure: ± 10 mm in both transverse directions and -27 and $+35$ mm from the geometrical focus on the axis [46].

Simulation and measurement results extracted from the 2-D data in Fig. 7 are presented in Fig. 8. Fig. 8(a) shows the envelope of the pressure amplitudes at the foci, electronically steered along the array axis, z . In addition, this plot shows the results of individual field scans when the focus is placed prefocally at -14 mm, at the focus, and postfocally at $+10$ mm. Similar data are presented in both Fig. 8(b) and (c) with envelopes for lateral focus steering and individual field scans in the focal plane $z = 120$ mm corresponding to the off-axis steered focus positions at -6 , 0 , and $+6$ mm. The data are normalized by the corresponding maximum values in the plots. The locations for the off-nominal focus scans were chosen at the pressure drop to 90% level (or 80% power level), as this is a common choice for setting focus steering limits in HIFU array systems for potential compensation [32]. Overall, simulation results are in good agreement with the measurements.

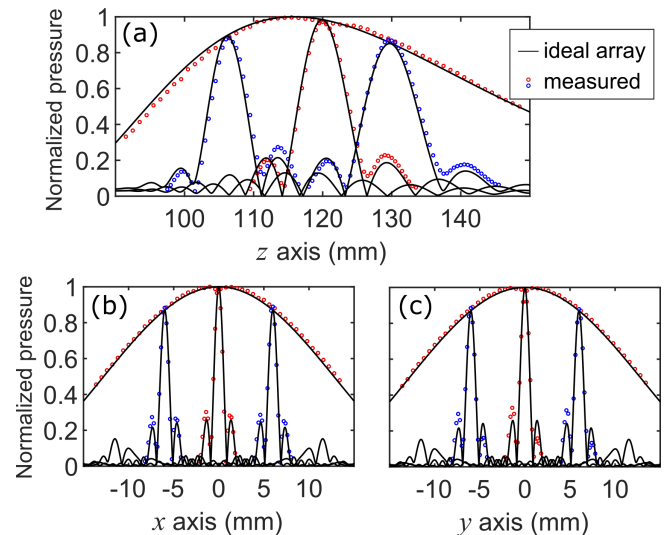


Fig. 8. Measurements (dots) and simulations (solid curves) showing pressure envelopes and selected scans within each envelope for focus steering of the array in the linear regime. Low-pressure (< 2 MPa) hydrophone scans were performed along each axis and normalized to the maximum achievable level. (a) Pressure scans along the axial direction (z -axis) for the cases of prefocal steering (-14 mm), postfocal steering ($+10$ mm), and no steering. Transverse pressure scans along (b) x -axis (horizontal) and (c) y -axis (vertical), for the cases of steered ± 6 mm and nonsteered foci. The ± 6 -mm transverse steering locations correspond to 90% of the maximum pressure. The top enveloping line corresponds to the maximum pressure for each steered location. The solid curves correspond to the simulated normalized pressure for an ideal array.

Electronic steering of the focus of the HIFU array at low driving voltages (i.e., for linear beam focusing conditions) brings about changes in the size, shape, and relative pressures of the focal region. As shown in Fig. 8(b) and (c), lateral steering of the focus in the geometric focal plane introduces a drop in the pressure amplitude but does not change the beam pattern, which is expected, as the effective F-number of the array does not change. On the contrary, steering the focus along the beam axis results in the change of both the pressure amplitude and the length of the focal lobe of the beam due to the associated change in the effective F-number of the array [see Fig. 8(a)]. Especially, the length of the focal lobe is reduced from 7.2 mm for the no steering case to 5.4 mm at the prefocal location and increased to 7.6 mm at the postfocal location (all at the -6 -dB level).

The effects of focus steering along the beam axis on nonlinear waveform distortion and shock formation are summarized in Fig. 9. Shown in Fig. 9(a) are the peak positive and negative pressures versus system driving voltage levels as measured for three steering conditions: without focus steering, at 14 -mm prefocal and 10 -mm postfocal. Prefocal and postfocal axial positions yield 90% of the maximum achievable pressure amplitude in the linear beam. The increase in the slope of the peak positive pressure curve indicates shock formation and begins at about the same voltage for no steering and postfocal conditions, with lower peak pressures at the postfocal location. For prefocal steering, higher voltage is necessary to reach shock-forming conditions, but peak pressures exceed those for postfocal conditions once the level of 19 – 20 V is reached. The peak negative pressure shows an almost linear trend for the entire range of voltage shown in all three cases.

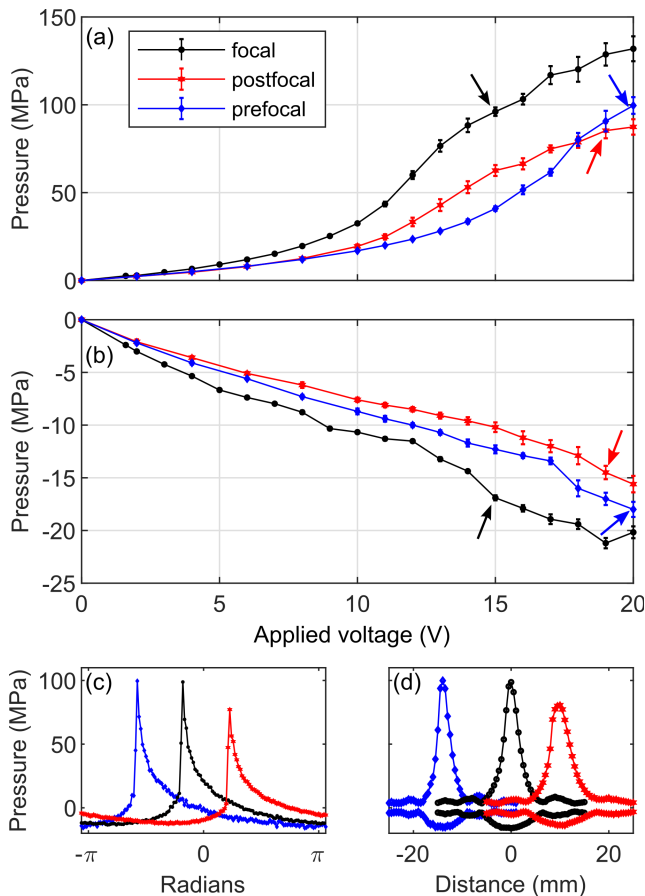


Fig. 9. (a) Peak positive and (b) peak negative focal pressures as functions of system driving voltage measured using a fiber optic hydrophone at different axial locations of the steered focus: -14 -mm prefocal (blue), nominal focus (black), and 10 -mm postfocal (red). The arrows indicate the voltage levels necessary to achieve a shock amplitude of 80 MPa for different steering locations (15 V for nominal focus, 20 V for prefocal, and 19 V for postfocal). (c) Corresponding focal pressure waveforms and (d) axial hydrophone scans through the focal regions showing peak positive and peak negative pressures for the different steering locations and the driving voltages indicated by arrows in Fig. 8(a) and (b).

Different behaviors of peak pressures for different focusing locations are driven by the change in the length of the focal lobe with steering (see Fig. 8). This, in turn, is determined by the change in the effective F-number. As shown in our previous studies [33], [47], the power output required for the formation of shocks at the focus and the corresponding amplitude of the fully developed shock increase for more focused transducers (lower F-number) and, thus, change when steering the focus axially. The effective F-numbers of the axially steered beams correspond to 0.74 , 0.83 , and 0.90 for the prefocal, focal, and postfocal locations, respectively.

The increase in the F-number for postfocal steering would require lower voltages for shock formation compared with the no steering case. However, the steering itself results in lower focal pressures. In combination, these two effects result in about the same voltages to reach shock-forming conditions for these two cases. For prefocal focusing, both stronger focusing and the drop in focal pressure due to steering result in higher voltages required for reaching shock-forming conditions. As nonlinear effects decrease the absolute value of

the peak negative pressures at the focus [48] and are delayed for more focused beams [47], for the same driving voltage, the peak negative pressure is the largest for the case of no steering and the smallest for the postfocal steering.

The arrows in Fig. 9(a) represent driving voltages required to generate shocks in water with about 80 -MPa amplitude necessary for initiating efficient BH (i.e., achieving boiling temperature in about the middle of 10 -ms pulses) at each steered focus position. Fig. 9(c) shows the focal waveforms collected with the corresponding driving voltage and steering. At the nominal focus, $p^+ = 98$ MPa and $p^- = -17$ MPa. For the prefocal -14 -mm steering location, 20 V was required to reach the same shock amplitude with $p^+ = 100$ MPa and $p^- = -18$ MPa. For both nominal focus and prefocal steering, the shock is not yet fully developed, i.e., its bottom pressure is above zero, and shock amplitude is smaller than the peak positive pressure. The postfocal $+10$ -mm location required 19 V with $p^+ = 85$ MPa and $p^- = -14.5$ MPa. The shock is fully developed in the postfocal location, but peak pressures in the waveform are smaller than for the cases of no-steering and prefocal steering.

Axial distributions of the peak positive and peak negative pressures for the three axially steered foci are shown in Fig. 9(d) for the same driving levels as in Fig. 9(c). While the length of the focal lobes for the peak negative pressure remains similar to that in the linear beam, it is substantially smaller for the peak positive pressure: 3.5 mm for no steering, 4.3 mm for postfocal, and 3 mm for prefocal steering (at the -6 -dB level).

The measurements of peak positive and negative focal pressures versus system driving voltage performed at the nominal focus and a focus location laterally steered by 6 mm (90% pressure amplitude level in the linear beam) are shown in Fig. 10(a) and (b). Similar to the axial focal steering case, at any given voltage, peak pressures are lower for the steered cases, and shock formation occurs at a higher voltage. However, unlike the axial steering case, this difference can be completely compensated for by scaling the system driving voltage by a factor of 0.9 [steered/adjusted curve in Fig. 10(a) and (b)] to compensate for the decrease in effective focusing gain as in the linear steering case [see Fig. 8(b) and (c)]. Thus, by increasing the voltage at the steered location, it was possible to achieve the same shock amplitude and peak pressures as for the nonsteered focus. Indeed, the focal waveform with a shock amplitude of 80 MPa recorded at the laterally steered location at 17 V was equivalent to the one collected without steering at 15 V [see Fig. 10(c)]. The beam pattern in the lateral direction [see Fig. 10(d)] also did not change with steering, similar to the linear case. The width of the focal lobe is similar to that in the linear beam for the peak negative pressure, but it is 0.4 mm smaller for the peak positive pressure, as expected [6].

D. Polyacrylamide Gel Experiments

The free-field measurements of the acoustic field under shock forming conditions provided estimates of the system driving voltages necessary for generating shocks with amplitudes sufficient for BH at the various steered focal locations. Especially, according to the previous studies, the time to reach boiling in polyacrylamide gel at 1.5 MHz with 80 -MPa shocks

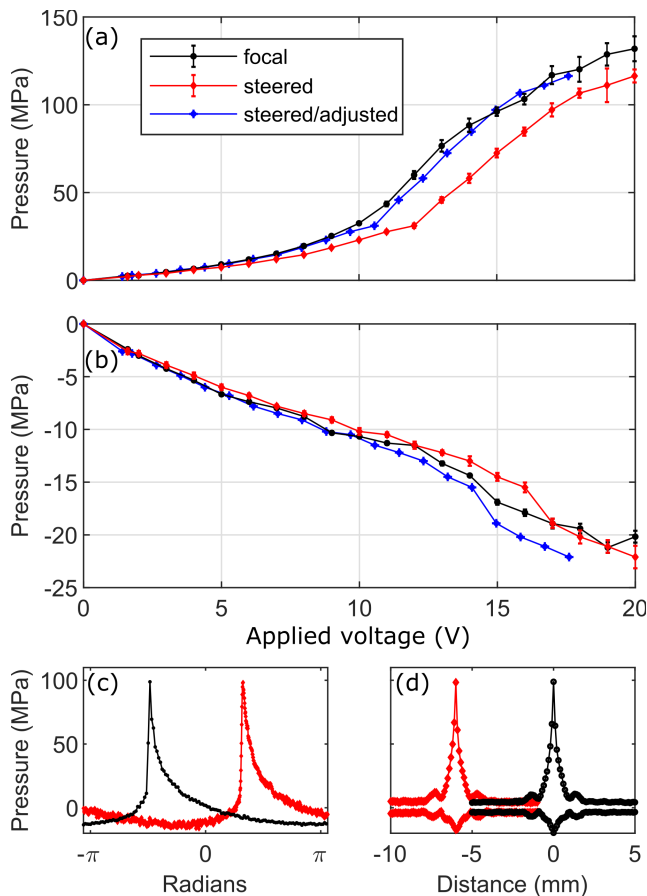


Fig. 10. (a) Peak positive and (b) peak negative focal pressures as functions of system driving voltage measured using a fiber optic hydrophone at the nominal focus (black) and at a focal position transversely steered by 6 mm (red). An adjusted curve (blue) for the steered location is also presented, for which the driving voltage is scaled by a factor of 0.9. This adjusted curve corresponds well to that obtained at the nominal focus. (c) Focal pressure waveforms at the voltage levels necessary to achieve 80-MPa shocks: 15 V for nominal focus and 17-V input for the steered position. (d) Transverse hydrophone scans through the focal regions showing peak positive and peak negative pressures for the nominal (at 15 V) and 6-mm steered (at 17 V) locations.

is 5 ms—half of the 10-ms BH pulse duration—which is appropriate for successful lesion formation [1], [40], [33]. The experiments in polyacrylamide gel phantoms were performed to confirm and tune these estimates if necessary; the results are represented in Fig. 11. Although somewhat subjective, it was determined that the voltage level was high enough for performing BH if an opaque region of disrupted gel structure consistently is formed at the focus within five delivered 10-ms pulses. Fig. 11(a) shows a representative cross section of a gel that has five different BH exposures delivered to the nominal focus of the HIFU array, labeled with the corresponding system voltage level. The top lesion labeled 14.9 V, although visually obvious, was not considered to be meeting the threshold criteria, as it did not form consistently at every attempted location. The second and third lesions labeled 15 V were formed consistently and also visibly larger and more pronounced; thus, they were considered to meet the threshold criteria, in agreement with hydrophone measurement-based estimates. The fourth and fifth lesions labeled 15.5 V are

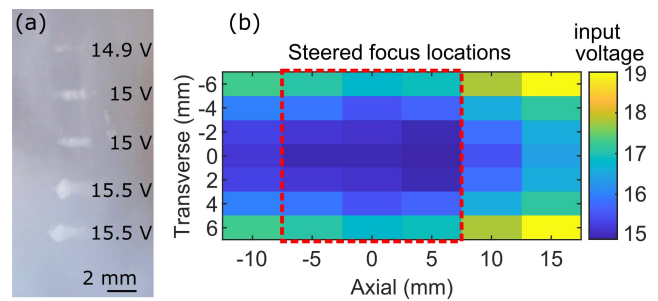


Fig. 11. (a) Representative photograph of a cross section of polyacrylamide gel showing five locations exposed to five 10-ms BH pulses delivered at 1-Hz PRF at escalating driving voltages. (b) Adjustment map of driving voltages of the Verasonics system for performing BH exposures in polyacrylamide gel with focus steering. This map represents the voltages necessary to induce BH in polyacrylamide gel with 10-ms pulses for given transverse and axial steering positions. The red box represents the practical steering range that was determined and used for subsequent volumetric gel exposures and *ex vivo* tissue ablation.

TABLE II

APPLIED VOLTAGE IN GEL/LIVER VOLUMETRIC BH TREATMENTS

Radial position (mm)	Prefocal: -5 mm voltage (V)	In plane: 0 mm voltage (V)	Postfocal: +5 mm voltage (V)
0.0	15.0 / 16.9	15.0 / 17.7	15.0 / 18.3
2.0	15.2 / 17.1	15.1 / 17.8	15.1 / 18.4
4.0	15.9 / 17.9	15.5 / 18.3	15.7 / 19.2
6.0	17.1 / 19.3	16.8 / 19.8	16.9 / 20.6

shown for comparison; the lesions are even larger and clearly exceeding the threshold criteria for BH, as expected.

The above-described procedure was then used to measure the BH threshold at each combined lateral and axial steering location [see Fig. 11(b)]. The locations for which the hydrophone measurements and corresponding estimations of time to boiling were available showed good agreement of predictions to the observed thresholds (see Table II). Based on these observations, the practical range was defined for focus steering corresponding to less than 14% increase in the system driving voltage (similar to linear steering range considerations): -5 to 5 mm steering axially and up to 6 mm laterally. Although this range would be larger if steering along with individual directions separately, the combination of axial and transverse steering required higher voltages.

Once the BH voltage thresholds were determined for all individual steering locations, BH exposures with the corresponding voltages were delivered to three planes (focal and 5-mm prefocal and postfocal). Trajectories within each plane comprised concentric circles with 2-mm spacing between the sonication points. The schematic of this trajectory is shown in Fig. 12, along with a photograph of the resulting lesion pattern in the gel. Some variation in the appearance of lesions in Fig. 12(b) is due to nonuniform lighting. The voltage values used for each concentric ring for all of the axial locations are presented in Table II.

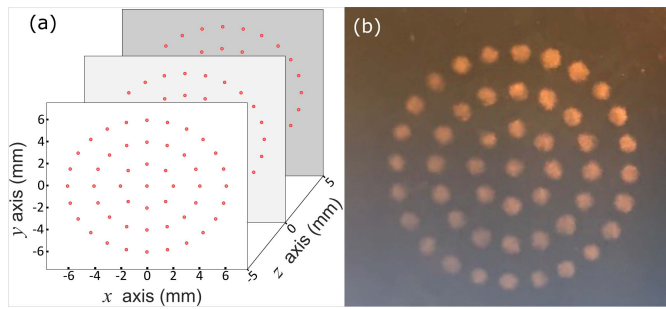


Fig. 12. (a) Focus steering pattern for a circular trajectory repeated in three layers. The spacing between points within the layer was 2 mm (as shown) or 1 mm, and 5-mm spacing between layers. (b) Photograph of a polyacrylamide gel exposed to the BH protocol along the circular trajectory with 2-mm spacing and 30 pulses per point.

E. Volumetric Liver Ablations

The initial, individual focus BH exposures of *ex vivo* liver showed that the voltage levels necessary for initiation of BH corresponded well to those estimated by derating the threshold levels for the gel to a specific depth in tissue to account for HIFU attenuation. Spot-checking focal steering positions within the imaging plane of the US probe showed bright hyperechoic regions in the US images indicating initiation of boiling. The corresponding threshold voltage levels were increased by 10% across the board for use in volumetric BH treatment (see Table II), similar to the approach taken in our previous experiments [11], [33]. The volumetric BH exposures of liver samples were then performed for circular trajectories with 2-mm spacing, in three axial planes steered at -5 , 0 , and $+5$ mm from the nominal focus of the array [see Fig. 12(a)]. Each focus location received 30 BH pulses. A representative liver sample bisected after the exposure is shown in Fig. 13(a) and (c); as seen, uniform BH lesions were formed at all steered locations, but the individual lesions did not merge.

Subsequently, a trajectory with 1-mm spacing between points was implemented and applied to liver samples. Each focus location received ten pulses. A representative bisected lesion before and after the flushing of the liquid contents is shown in Fig. 13(b) and (d), respectively. In this sample, the individual lesions appear to have merged such that no intact liver tissue was observed within the lesion volume. However, the connective tissue structure that remained within the lesion was clearly visible and similar in appearance to that observed in our previous studies of volumetric BH ablation [9]. The lateral boundaries of the volume had a clear and distinct demarcation. The gross analysis showed no apparent thermal damage, as there was no discoloration in the tissue at the boundary as is typical for treatments with a thermal component.

Additional BH exposures with 1-mm in-plane spacing and fewer pulses per point (especially, 5 and 1) were subsequently performed to determine the minimal BH “dose” that would provide uniform volumetric liquefaction. The lesion that formed with five pulses per location appeared very similar to that with ten pulses per location [as shown in Fig. 13(b) and (d)], in which all the lesions merged and the only remaining material appeared to be connective tissue. The exposure with one pulse per location resulted in only

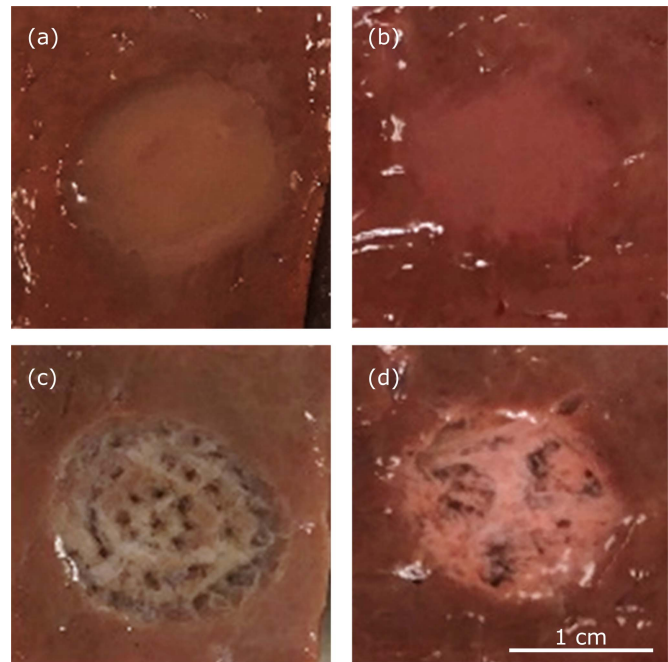


Fig. 13. Representative photographs of volumetric *ex vivo* bovine liver after BH treatment. (a) and (b) Before and (c) and (d) after the liquid contents have been flushed out. (a) and (c) 2-mm spaced trajectory consisting of 49 points per layer and 30 pulses per point. (b) and (d) 1-mm spaced trajectory consisting of 136 points per layer and 10 pulses per point.

partial liquefaction/disruption of the treated volume, as the individual lesions were too small to merge.

IV. DISCUSSION

This article presents the development, acoustic characterization, and *ex vivo* testing of a US-guided Verasonics-based BH system designed for the treatment of abdominal targets, e.g., tumors in the liver, kidney, and pancreas. A 256-element HIFU array was matched to the custom-modified Verasonics system to enable electronic steering for generating volumetric lesions. Modifications to the driving hardware and software of the Verasonics system were introduced to enable the delivery of 10-ms long pulses with a sustained amplitude that would initiate boiling of the target tissue within several milliseconds. The range of electronic focus steering with equalized nonlinear exposure conditions, which could feasibly be used to generate volumetric BH lesions, was investigated in the lateral and axial dimensions. Conservatively, this range was determined to be ± 6 mm radially and ± 5 mm axially from the nominal focus. By measuring and modeling the acoustic output in water, it was possible to estimate the system driving voltages necessary to treat all of the desired focus locations with BH. These estimations were followed by implementing and testing automated BH treatment routines in transparent polyacrylamide gel phantoms, where all the desired focus steering locations could be treated using the corresponding driving voltages. The phantoms allowed for visual confirmation of the BH lesion formation. Ultimately, the volumetric BH treatment routines were implemented in *ex vivo* bovine liver samples. These tests showed that achieving uniform volumetric tissue liquefaction required that individual focus locations had to

be spaced no more than 1 mm laterally and 5 mm axially, and at least, five BH pulses had to be delivered per focal point. The overall liquefied volume was 3.5 mL, and the total treatment time was 34 min. The maximum driving voltage used (20.9 V) was 48% of the maximum voltage of 43 V that can be tolerated by the HIFU array. This power surplus appears sufficient to compensate for attenuation losses *in vivo* in the intervening tissues if aberration compensation strategies are employed [11]. The associated studies are currently underway.

Various challenges have been addressed in building the BH prototype. The modifications to the Verasonics system required the addition of seven capacitors in parallel with the dc power supply to meet the energy requirements. Furthermore, software modifications were needed to account for the changes in the system hardware configuration and allow for the longer sustained output without damaging any of the existing components. Ultimately, the system was capable of delivering 3.7-kW electric power (2.2-kW acoustic power) to the transducer in 10-ms bursts. Note that this limitation in peak power was dictated by the safety concerns for the internal components of the Verasonics in the case of relatively long 10-ms pulses, not the safety limits of the HIFU array. This limitation is not applicable to bursts 5 ms in duration or shorter; therefore, larger power outputs could be used with shorter bursts. Once the capabilities of the Verasonics system were upgraded, scripts were developed that could control the steering and the output power for each of the target locations.

To facilitate rapid changes in driving voltage when steering to different focal positions, two strategies were initially implemented. In the first strategy, a maximum input driving voltage on each element was kept constant for all sonication points, and the pulsewidth modulation (PWM) method was used to alter the effective voltage on the elements to reduce the output power of the array for central steering locations [26]. In the second strategy, the dc system driving voltage was directly changed for each steering location, which was feasible within the relatively long 1-s OFF-time between the BH pulses used here. This strategy had the same desired effect on acoustic output as the modulation of the pulsewidth. However, if a higher PRF were to be used, the first strategy would be taken, where the changes can occur faster—within milliseconds.

Linear simulations and measurements showed the ability of the array to steer up to -14 and $+10$ mm axially from the nominal focus and ± 6 mm transversely in the focal plane, with a 10% drop in pressure or 20% drop in acoustic intensity at the maximum steering locations. With up to 10% voltage compensation by the system, the same pressures can be achieved over this entire steering region. Nonlinear acoustic measurements confirmed the ability of the array to generate shock fronts of 80 MPa sufficient for initiating BH in the same region. In transverse steering, the same compensation in the driving voltage was necessary for both linear and shock-forming focusing conditions. However, significantly higher compensation was necessary to reach the same shock amplitude when steering axially: 33% at -14 -mm and 26% at $+10$ -mm steering locations. In gel and liver experiments, therefore, only ± 5 -mm axial steering was implemented.

There were a number of considerations taken into account for limiting the practical steering range by ± 5 mm axially. Due to the change in the effective F-number of the HIFU array when steering axially, the pressure amplitude necessary to begin developing shocks is higher when steering prefocally than at the focus or postfocally [33]. The higher required amplitude also increases the likelihood of prefocal cavitation and associated shielding effects [33]. Furthermore, sufficient power headroom will be needed to compensate for attenuation in the propagation path for future transcatheter treatments *in vivo*.

It was initially assumed in this work that, similar to the experiments in *ex vivo* liver with the Sonalleve V1 system at 1.2 MHz, a 2-mm spacing between the focal points in the circular trajectory would cause the BH lesions to fully merge [9]. However, due to the higher frequency of 1.5 MHz and lower F-number of the array, a trajectory with 1-mm spacing was necessary to achieve full mechanical ablation of the target volume. This change in trajectory increased the number of treatment locations per axial plane to 136 from the 49 locations for 2-mm spacing. However, uniform liquefaction was achieved with only five pulses, as opposed to 30 pulses per location in the 2-mm-spaced trajectory. This actually reduced the treatment time for the volume from 73 to 34 min in this study.

In fact, there are several ways to accelerate the treatment rate. Further optimization of spacing between lesions could lead to fewer treatment locations or delivery of fewer BH pulses per location. Another approach is to slightly increase the pulse average acoustic power, reduce the time to reach boiling, reduce the BH pulse duration accordingly, and increase the PRF to maintain the same duty cycle [11], [33]. Because lesion size was previously shown to depend on the number of BH pulses delivered rather than on the total “HIFU on” time per location, the decrease in the pulselength combined with an increase in PRF by up to tenfold would cause proportional acceleration of the ablation rate [38]. Furthermore, slightly increasing the duty cycle (e.g., up to 2%–3% from the current 1%) and, therefore PRF would also accelerate treatment another twofold to threefold although care should be taken to not induce thermal buildup in the tissue volume.

While the developed array with circular elements has a fairly high filling factor of about 60%, recently, even more compact almost fully populated quasi-random arrays have been developed, which gives a potential for achieving more power and operating at higher shock-amplitude levels within given limitations of the intensity at the array surface [46], [49]. However, with given dimensions of the array and the number of its elements, an increased filling factor would result in increased dimensions and directivity of each element, thus reducing the steering capabilities of the array. A larger number of elements would then be necessary to maintain the same steering range.

In the current implementation of volumetric BH treatments, the focus was steered in circular trajectories that only partially lay within the imaging plane of the coaxial US probe. As a result, echogenic bubbles could not be visualized when steering further than 2 mm off the imaging plane. This presented an

important drawback to implementing any US imaging-based algorithm for real-time feedback on the completeness of ablation. Therefore, in future studies with the current system, the steering trajectory in each plane will be altered to only include points within 2 mm of the US imaging plane and will be rectangular (as opposed to circular) in shape. Further efforts will be directed toward US imaging using 1.5-D or 2-D arrays with steering capability in the elevational plane or developing a dual-purpose array, both for therapy and imaging, to provide imaging guidance for larger treatment volumes.

V. CONCLUSION

A preclinical prototype for transcutaneous US-guided mechanical ablation of liver and kidney using the BH approach was developed. A 256-element, 1.5-MHz phased-array HIFU transducer was designed and implemented with Verasonics-based driving electronics. The array was capable of electronically steering US waves with high-amplitude shocks (>80 MPa) to mechanically liquefy tissue volumes in *ex vivo* liver samples. It was shown that a 10-ms duration, 1-Hz PRF pulsing protocol could reliably generate volumes of liquefied tissue of approximately 3.5 cm³ (2 cm axially and 1.5 cm laterally) spanning the depth of 5–25 mm below the tissue surface when operating at only 16% of the maximum achievable power of the array and, thus, allowing for more than sixfold power increase to compensate for tissue attenuation when focusing at clinically relevant depths. In this sonication protocol, the focus was steered to locations at three axial depths of 5 mm apart with a lateral spacing at each depth of 1 mm; with five pulses per location and a total of 2040 pulses per volume, the treatment time was 34 min. Future studies will investigate options for accelerating the treatment, extending the treatment volume, developing US imaging-based feedback approaches, and aberration correction protocols. In spite of the need for these improvements, this study has shown that this newly developed HIFU system should be capable, in terms of the power achievable, of delivering BH pulses in preclinical *in vivo* studies.

ACKNOWLEDGMENT

The authors are grateful to Peter Kaczkowski and Adam Maxwell for help in modifying a Verasonics system.

REFERENCES

- [1] T. D. Khokhlova, M. S. Canney, V. A. Khokhlova, O. A. Sapozhnikov, L. A. Crum, and M. R. Bailey, "Controlled tissue emulsification produced by high intensity focused ultrasound shock waves and millisecond boiling," *J. Acoust. Soc. Amer.*, vol. 130, no. 5, pp. 3498–3510, Nov. 2011.
- [2] K. J. Pahk, G. H. Mohammad, M. Malago, N. Saffari, and D. K. Dhar, "A novel approach to ultrasound-mediated tissue decellularization and intra-hepatic cell delivery in rats," *Ultrasound Med. Biol.*, vol. 42, no. 8, pp. 1958–1967, 2016.
- [3] M. Hoogenboom *et al.*, "Impact of MR-guided boiling histotripsy in distinct murine tumor models," *Ultrasound Med. Biol.*, vol. 38, pp. 1–8, Sep. 2017.
- [4] V. A. Khokhlova *et al.*, "Histotripsy methods in mechanical disintegration of tissue: Towards clinical applications," *Int. J. Hyperthermia*, vol. 31, no. 2, pp. 145–162, Feb. 2015.
- [5] V. A. Khokhlova, M. R. Bailey, J. A. Reed, B. W. Cunitz, P. J. Kaczkowski, and L. A. Crum, "Effects of nonlinear propagation, cavitation, and boiling in lesion formation by high intensity focused ultrasound in a gel phantom," *J. Acoust. Soc. Amer.*, vol. 119, no. 3, pp. 1834–1848, 2006.
- [6] M. S. Canney, V. A. Khokhlova, O. V. Bessonova, M. R. Bailey, and L. A. Crum, "Shock-induced heating and millisecond boiling in gels and tissue due to high intensity focused ultrasound," *Ultrasound Med. Biol.*, vol. 36, no. 2, pp. 250–267, Feb. 2010.
- [7] J. C. Simon, O. A. Sapozhnikov, V. A. Khokhlova, Y.-N. Wang, L. A. Crum, and M. R. Bailey, "Ultrasonic atomization of tissue and its role in tissue fractionation by high intensity focused ultrasound," *Phys. Med. Biol.*, vol. 57, no. 23, pp. 8061–8078, Dec. 2012.
- [8] K. J. Pahk, P. Gélat, D. Sinden, D. K. Dhar, and N. Saffari, "Numerical and experimental study of mechanisms involved in boiling histotripsy," *Ultrasound Med. Biol.*, vol. 43, no. 12, pp. 2838–2861, 2017.
- [9] Y.-N. Wang *et al.*, "Mechanical decellularization of tissue volumes using boiling histotripsy," *Phys. Med. Biol.*, vol. 63, no. 23, Dec. 2018, Art. no. 235023.
- [10] T. D. Khokhlova *et al.*, "Ultrasound-guided tissue fractionation by high intensity focused ultrasound in an *in vivo* porcine liver model," *Proc. Nat. Acad. Sci. USA*, vol. 111, no. 22, pp. 8161–8166, Jun. 2014.
- [11] T. D. Khokhlova *et al.*, "Pilot *in vivo* studies on transcutaneous boiling histotripsy in porcine liver and kidney," *Sci. Rep.*, vol. 9, no. 1, Dec. 2019, Art. no. 20176.
- [12] V. A. Khokhlova *et al.*, "A novel method for non-invasive mechanical ablation of prostate tumors using pulsed focused ultrasound," *Urologia*, vol. 6, pp. 67–73, Dec. 2019.
- [13] T. Looi, V. Khokhlova, K. Hynynen, and J. Drake, "A preliminary *in vivo* porcine study of long pulse histotripsy for thrombolysis of intraventricular hemorrhagic clot," *J. Acoust. Soc. Am.*, vol. 140, no. 4, p. 3031, 2016.
- [14] M. Hoogenboom, D. Eikelenboom, M. H. den Brok, A. Heerschap, J. J. Fütterer, and G. J. Adema, "Mechanical high-intensity focused ultrasound destruction of soft tissue: Working mechanisms and physiologic effects," *Ultrasound Med. Biol.*, vol. 41, no. 6, pp. 1500–1517, Jun. 2015.
- [15] G. R. Schade, Y.-N. Wang, S. D'Andrea, J. H. Hwang, W. C. Liles, and T. D. Khokhlova, "Boiling histotripsy ablation of renal cell carcinoma in the eker rat promotes a systemic inflammatory response," *Ultrasound Med. Biol.*, vol. 45, no. 1, pp. 137–147, Jan. 2019.
- [16] K. J. Pahk *et al.*, "Boiling histotripsy-induced partial mechanical ablation modulates tumour microenvironment by promoting immunogenic cell death of cancers," *Sci. Rep.*, vol. 9, no. 1, Dec. 2019, Art. no. 9050.
- [17] J. R. Chevillet *et al.*, "Release of cell-free MicroRNA tumor biomarkers into the blood circulation with pulsed focused ultrasound: A noninvasive, anatomically localized, molecular liquid biopsy," *Radiology*, vol. 283, no. 1, pp. 158–167, Apr. 2017.
- [18] T. D. Khokhlova, W. L. Monsky, Y. A. Haider, A. D. Maxwell, Y.-N. Wang, and T. J. Matula, "Histotripsy liquefaction of large hematomas," *Ultrasound Med. Biol.*, vol. 42, no. 7, pp. 1491–1498, Jul. 2016.
- [19] A. Partanen, M. Tillander, P. S. Yarmolenko, B. J. Wood, M. R. Dreher, and M. O. Köhler, "Reduction of peak acoustic pressure and shaping of heated region by use of multifoci sonications in MR-guided high-intensity focused ultrasound mediated mild hyperthermia," *Med. Phys.*, vol. 40, no. 1, Dec. 2012, Art. no. 013301.
- [20] K. Hynynen and R. M. Jones, "Image-guided ultrasound phased arrays are a disruptive technology for non-invasive therapy," *Phys. Med. Biol.*, vol. 61, no. 17, pp. R206–R248, Sep. 2016.
- [21] J. J. Macoskey *et al.*, "Soft-tissue aberration correction for histotripsy," *IEEE Trans. Ultrason., Ferroelectr., Freq. Control*, vol. 65, no. 11, pp. 2073–2085, Nov. 2018.
- [22] M. Schwenke *et al.*, "A focused ultrasound treatment system for moving targets (part I): Generic system design and in-silico first-stage evaluation," *J. Therapeutic Ultrasound*, vol. 5, no. 1, p. 20, Dec. 2017.
- [23] H. Wang, E. S. Ebbini, M. O'Donnell, and C. A. Cain, "Phase aberration correction and motion compensation for ultrasonic hyperthermia phased arrays: Experimental results," *IEEE Trans. Ultrason., Ferroelectr., Freq. Control*, vol. 41, no. 1, pp. 34–43, Jan. 1994.
- [24] A. Diodato, A. Cafarelli, A. Schiappacasse, S. Tognarelli, G. Ciuti, and A. Menciasci, "Motion compensation with skin contact control for high intensity focused ultrasound surgery in moving organs," *Phys. Med. Biol.*, vol. 63, no. 3, Jan. 2018, Art. no. 035017.
- [25] V. A. Khokhlova *et al.*, "Design of HIFU transducers to generate specific nonlinear ultrasound fields," *Phys. Procedia*, vol. 87, pp. 132–138, 2016.
- [26] M. A. Ghanem *et al.*, "Field characterization and compensation of vibrational nonuniformity for a 256-element focused ultrasound phased array," *IEEE Trans. Ultrason., Ferroelectr., Freq. Control*, vol. 65, no. 9, pp. 1618–1630, Sep. 2018.

- [27] M. Pernot, J.-F. Aubry, M. Tanter, J.-L. Thomas, and M. Fink, "High power transcranial beam steering for ultrasonic brain therapy," *Phys. Med. Biol.*, vol. 48, no. 16, pp. 2577–2589, Aug. 2003.
- [28] J. W. Hand, A. Shaw, N. Sadhoo, S. Rajagopal, R. J. Dickinson, and L. R. Gavrilov, "A random phased array device for delivery of high intensity focused ultrasound," *Phys. Med. Biol.*, vol. 54, no. 19, pp. 5675–5693, Oct. 2009.
- [29] J. Tavakkoli, A. Birer, A. Arefiev, F. Prat, J.-Y. Chapelon, and D. Cathignol, "A piezocomposite shock wave generator with electronic focusing capability: Application for producing cavitation-induced lesions in rabbit liver," *Ultrasound Med. Biol.*, vol. 23, no. 1, pp. 107–115, Jan. 1997.
- [30] D. N. Stephens, D. E. Kruse, S. Qin, and K. W. Ferrara, "Design aspects of focal beams from high-intensity arrays," *IEEE Trans. Ultrason., Ferroelectr., Freq. Control*, vol. 58, no. 8, pp. 1590–1602, Aug. 2011.
- [31] G. Pinton, J.-F. Aubry, and M. Tanter, "Direct phase projection and transcranial focusing of ultrasound for brain therapy," *IEEE Trans. Ultrason., Ferroelectr., Freq. Control*, vol. 59, no. 6, pp. 1149–1159, Jun. 2012.
- [32] W. Kreider *et al.*, "Characterization of a multi-element clinical HIFU system using acoustic holography and nonlinear modeling," *IEEE Trans. Ultrason., Ferroelectr., Freq. Control*, vol. 60, no. 8, pp. 1683–1698, Aug. 2013.
- [33] P. B. Rosnitskiy *et al.*, "Design of HIFU transducers for generating specified nonlinear ultrasound fields," *IEEE Trans. Ultrason., Ferroelectr., Freq. Control*, vol. 64, no. 2, pp. 374–390, Feb. 2017.
- [34] O. A. Sapozhnikov, Y. A. Pishchal'nikov, and A. V. Morozov, "Reconstruction of the normal velocity distribution on the surface of an ultrasonic transducer from the acoustic pressure measured on a reference surface," *Acoust. Phys.*, vol. 49, no. 3, pp. 354–360, May 2003.
- [35] O. A. Sapozhnikov, S. A. Tsysar, V. A. Khokhlova, and W. Kreider, "Acoustic holography as a metrological tool for characterizing medical ultrasound sources and fields," *J. Acoust. Soc. Amer.*, vol. 138, no. 3, pp. 1515–1532, Sep. 2015.
- [36] P. V. Yuldashev and V. A. Khokhlova, "Simulation of three-dimensional nonlinear fields of ultrasound therapeutic arrays," *Acoust. Phys.*, vol. 57, no. 3, pp. 334–343, May 2011.
- [37] *T-Array—Therapeutic Array Simulator*. Accessed: 2015. [Online]. Available: <http://limu.msu.ru/product/3124/home?language=en>
- [38] T. D. Khokhlova, Y. A. Haider, A. D. Maxwell, W. Kreider, M. R. Bailey, and V. A. Khokhlova, "Dependence of boiling histotripsy treatment efficiency on HIFU frequency and focal pressure levels," *Ultrasound Med. Biol.*, vol. 43, no. 9, pp. 1975–1985, Sep. 2017.
- [39] C. Lafon *et al.*, "Gel phantom for use in high-intensity focused ultrasound dosimetry," *Ultrasound Med. Biol.*, vol. 31, no. 10, pp. 1383–1389, Oct. 2005.
- [40] O. V. Bessonova, V. A. Khokhlova, M. S. Canney, M. R. Bailey, and L. A. Crum, "A derating method for therapeutic applications of high intensity focused ultrasound," *Acoust. Phys.*, vol. 56, no. 3, pp. 354–363, May 2010.
- [41] A. D. Maxwell *et al.*, "A prototype therapy system for transcutaneous application of boiling histotripsy," *IEEE Trans. Ultrason., Ferroelectr., Freq. Control*, vol. 64, no. 10, pp. 1542–1557, Oct. 2017.
- [42] F. A. Duck, *Physical Properties of Tissues: A Comprehensive Reference Book*. New York, NY, USA: Academic, 1990.
- [43] Y. Jing, D. Shen, and G. T. Clement, "Verification of the westervelt equation for focused transducers," *IEEE Trans. Ultrason., Ferroelectr., Freq. Control*, vol. 58, no. 5, pp. 1097–1101, May 2011.
- [44] A. D. Maxwell, C. A. Cain, T. L. Hall, J. B. Fowlkes, and Z. Xu, "Probability of cavitation for single ultrasound pulses applied to tissues and tissue-mimicking materials," *Ultrasound Med. Biol.*, vol. 39, no. 3, pp. 449–465, Mar. 2013.
- [45] L. R. Gavrilov and J. W. Hand, "A theoretical assessment of the relative performance of spherical phased arrays for ultrasound surgery," *IEEE Trans. Ultrason., Ferroelectr., Freq. Control*, vol. 47, no. 1, pp. 125–139, Jan. 2000.
- [46] P. B. Rosnitskiy, B. A. Vysokanov, L. R. Gavrilov, O. A. Sapozhnikov, and V. A. Khokhlova, "Method for designing multielement fully populated random phased arrays for ultrasound surgery applications," *IEEE Trans. Ultrason., Ferroelectr., Freq. Control*, vol. 65, no. 4, pp. 630–637, Apr. 2018.
- [47] P. B. Rosnitskiy, P. V. Yuldashev, and V. A. Khokhlova, "Effect of the angular aperture of medical ultrasound transducers on the parameters of nonlinear ultrasound field with shocks at the focus," *Acoust. Phys.*, vol. 61, no. 3, pp. 301–307, May 2015.
- [48] O. V. Bessonova, V. A. Khokhlova, M. R. Bailey, M. S. Canney, and L. A. Crum, "Focusing of high power ultrasound beams and limiting values of shock wave parameters," *Acoust. Phys.*, vol. 55, nos. 4–5, pp. 463–473, Oct. 2009.
- [49] P. Ramaekers, M. de Greef, R. Berriet, C. T. W. Moonen, and M. Ries, "Evaluation of a novel therapeutic focused ultrasound transducer based on Fermat's spiral," *Phys. Med. Biol.*, vol. 62, no. 12, pp. 5021–5045, Jun. 2017.



Christopher R. Bawiec received the B.S. degree in electrical and computer engineering from the University of Colorado at Boulder, Boulder, CO, USA, in 2005, and the Ph.D. degree in biomedical engineering from Drexel University, Philadelphia, PA, USA, in 2015.

He completed his postdoctoral training as a Whitaker Scholar at the Laboratory of Therapeutic Applications of Ultrasound (LabTAU), Lyon, France. He is currently a Senior Fellow with the University of Washington School of Medicine,

Seattle, WA, USA, where he is pursuing his research interests in therapeutic and diagnostic ultrasound.



Tatiana D. Khokhlova received the Ph.D. degree in physics from Moscow State University (MSU), Moscow, Russia, in 2008.

After graduation from the Ph.D. program, she moved to the University of Washington (UW), Seattle, WA, USA, for postdoctoral training at the Applied Physics Laboratory, and then completed a research fellowship at the Department of Medicine. She is currently a Research Associate Professor with the Department of Medicine, UW. Her research interests are in physical acoustics,

therapeutic ultrasound, and photoacoustic imaging.



Oleg A. Sapozhnikov received the M.S. degree in physics and the Ph.D. and D.Sc. degrees in acoustics from Moscow State University (MSU), Moscow, Russia, in 1985, 1988, and 2008, respectively.

He is currently a Professor with the Department of Acoustics, Physics Faculty, MSU. Since 1996, he has been with Applied Physics Laboratory, Center for Industrial and Medical Ultrasound, University of Washington, Seattle, WA, USA. His research interests are physical acoustics,

nonlinear wave phenomena, medical ultrasound including shock wave lithotripsy, high-intensity focused ultrasound, and ultrasound-based imaging.

Dr. Sapozhnikov has been a member of the Board of International Congress on Ultrasonics since 2009 and the Head of the Physical Ultrasound Division of the Scientific Council on Acoustics of the Russian Academy of Sciences since 2009.



Pavel B. Rosnitskiy received the M.S. degree in physics and the Ph.D. degree in acoustics from Moscow State University (MSU), Moscow, Russia, in 2016 and 2019, respectively.

He is currently a Junior Research Scientist with the Department of Medical Physics, Physics Faculty, MSU. His current research interests include nonlinear acoustics, ultrasound imaging, design of multielement arrays, and therapeutic applications of high-intensity focused ultrasound waves with shocks.

Dr. Rosnitskiy was awarded by scholarships named after R. V. Khokhlov and S. I. Vavilov by the Scholarship of the President of Russia from 2014 to 2016 and the International Student Award from the Acoustical Society of America in 2016 during his studies at MSU. He was also recognized for the Best Undergraduate Student Project in 2013, the Best M.S. Thesis in 2016, and the Best Student of the Physics Faculty at MSU in 2015.



Bryan W. Cunitz received the B.A. degree in physics from the Colby College, Waterville, ME, USA, in 1999, the B.S. degree in electrical engineering from the Dartmouth College, Hanover, NH, USA, in 2000, and the M.S. degree in electrical engineering from the University of Washington, Seattle, WA, USA, in 2005.

He is currently a Senior Research Engineer with Applied Physics Laboratory, Center for Industrial and Medical Ultrasound, University of Washington, where he is involved in improving

ultrasound systems for the detection of kidney stones, therapeutic applications of focused ultrasound for the breaking and repositioning of kidney stones, image-guided acoustic hemostasis, transducer development, and acoustic output measurements.



Mohamed A. Ghanem received the B.S. degree in civil engineering and the M.S. and Ph.D. degrees in aeronautics and astronautics engineering from the University of Washington, Seattle, WA, USA, in 2009, 2012, and 2018, respectively. He received his Engineer in Training Certificate from the State of Washington in 2009.

He was a Structural Engineer with SIE, Mukilteo, WA, USA, from 2012 to 2014. He is currently a Research Associate with Applied Physics Laboratory (APL), University of

Washington. Most of his work has been focused on linear and nonlinear finite element analysis. His research is focused on radiation force toward the development of 3-D acoustical traps for macroscopic objects and holographic beam shaping for medical applications.



Christopher Hunter received the B.S. degree in applied mathematics from the University of Washington, Seattle, WA, USA, in 2015.

He has been a Research Engineer with Applied Physics Laboratory (APL), Center for Industrial and Medical Ultrasound, University of Washington, since 2015. His research interests focus on ultrasound metrology and acoustic characterization of ultrasound transducers.



Wayne Kreider received the B.S. and M.S. degrees in engineering mechanics at Virginia Tech, Blacksburg, VA, USA, in 1993 and 1995, respectively, and the Ph.D. degree in bioengineering from the University of Washington, Seattle, WA, USA, in 2008.

He is a licensed Professional Engineer in the Commonwealth of Virginia. He was an Engineer with Naval Surface Warfare Center, Dahlgren, VA, USA, and Dominion Engineering Inc., Reston, VA, USA. Since 2001, he has been

with the Applied Physics Laboratory (APL), Center for Industrial and Medical Ultrasound, University of Washington. His research interests include acoustic cavitation, transport processes in oscillating bubbles, therapeutic ultrasound, and ultrasound metrology.



George R. Schade received the bachelor's and M.D. degrees from The University of Chicago, Chicago, IL, USA, in 2003 and 2007, respectively.

He then completed his Urology residency at the University of Michigan, Ann Arbor, MI, USA, where he developed an interest in therapeutic ultrasound. Following residency, he moved to the University of Washington, Seattle, WA, USA, where he completed a Society of Urologic Oncology Fellowship and then joined the Faculty as an

Assistant Professor with the Department of Urology. He is also a practicing Urologic Oncologist, aiming to develop diagnostic and therapeutic ultrasound to improve the care of patients with urologic cancers.



Petr V. Yuldashev received the M.S. degree in physics and the Ph.D. degree in acoustics from Moscow State University (MSU), Moscow, Russia, in 2008 and 2011, respectively, and the Ph.D. degree in acoustics from the École Centrale de Lyon (ECL), Écully, France, through the Double Ph.D. Program of the French Government.

After graduation from the Ph.D. program, he was appointed by Moscow State University, where he is currently an Associate Professor with the Department of General Physics and

Condensed Matter Physics, Physics Faculty. He is also with the Department of Fluid Mechanics, Acoustics, and Energetics, ECL, to work on the propagation of shock waves in a turbulent atmosphere and the utilization of nonlinear acoustics effects to calibrate high-frequency broadband microphones. His research interests pertain to nonlinear acoustics, shock wave focusing, nonlinear wave propagation in inhomogeneous media, sonic booms, nonlinear modeling, and shadowgraphy measurement methods for acoustic phenomena.



Vera A. Khokhlova received the M.S. degree in physics and the Ph.D. and D.Sc. degrees in acoustics from Moscow State University (MSU), Moscow, Russia, in 1986, 1991, and 2012, respectively.

After graduation from the Ph.D. program, she was appointed by the Moscow State University, where she is currently an Associate Professor with the Department of Acoustics, Physics Faculty. Since 1995, she has been with the Applied Physics Laboratory, Center for Industrial and

Medical Ultrasound, University of Washington, Seattle, WA, USA. Her research interests are in the field of nonlinear acoustics, therapeutic ultrasound, including metrology and bioeffects of high-intensity focused ultrasound fields, shock wave focusing, nonlinear wave propagation in inhomogeneous media, and nonlinear modeling.

Dr. Khokhlova has been a fellow of the Executive Council of the Acoustical Society of America since 2008. She was a member of the Executive Council of the Acoustical Society of America from 2012 to 2015 and the Board of the International Society for Therapeutic Ultrasound from 2004 to 2008 and 2011 to 2014. She has been a member of the Physical Ultrasound Division of the Scientific Council on Acoustics of the Russian Academy of Sciences since 2009. She has been an Associate Editor of the IEEE TUFFC since 2013.